Double Resonant Raman Scattering and Valley Coherence Generation in Monolayer WSe_2

G. Wang,[1] M. M. Glazov,[2,1] C. Robert,[1] T. Amand,[1] X. Marie,[1] and B. Urbaszek[1]
[1]*Université de Toulouse, INSA-CNRS-UPS, LPCNO, 135 avenue de Rangueil, 31077 Toulouse, France*
[2]*Ioffe Institute, 26 Polytechnicheskaya, 194021 St.-Petersburg, Russia*
(Received 22 May 2015; published 9 September 2015)

The electronic states at the direct band gap of monolayer transition metal dichalcogenides such as WSe_2 at the K^+ and K^- valleys are related by time reversal and may be viewed as pseudospins. The corresponding optical interband transitions are governed by robust excitons. Excitation with linearly polarized light yields the coherent superposition of exciton pseudospin states, referred to as coherent valley states. Here, we uncover how and why valley coherence can be generated efficiently. In double resonant Raman spectroscopy, we show that the optically generated $2s$ exciton state differs from the $1s$ state by exactly the energy of the combination of several prominent phonons. Superimposed on the exciton photoluminescence (PL), we observe the double resonant Raman signal. This spectrally narrow peak shifts with the excitation laser energy as incoming photons match the $2s$ and outgoing photons the $1s$ exciton transition. The multiphonon resonance has important consequences: following linearly polarized excitation of the $2s$ exciton, a superposition of valley states is efficiently transferred from the $2s$ to $1s$ state. This explains the high degree of valley coherence measured for the $1s$ exciton PL.

DOI: 10.1103/PhysRevLett.115.117401 PACS numbers: 78.60.Lc, 78.55.-m, 78.66.Li, 78.67.Pt

Introduction.—Monolayer (ML) transition metal dichalcogenides (TMDCs) such as MoS_2 and WSe_2 have a direct optical band gap at the K points of the Brillouin zone [1–3]. The strong light-matter interaction governed by robust excitons introduces ML TMDCs as flexible materials for optoelectronics [4]. Additional motivation for research on 2D excitons comes from the possibility to explore a new degree of freedom in condensed matter physics: the valley index in $\boldsymbol{k}$ space [5,6]. The electronic states in the K^+ and K^- valleys are related by time reversal and can be optically initialized using the chiral optical selection rules [5,6]. Hence, the valley degree of freedom can be manipulated in simple optical spectroscopy experiments [7,8], an opportunity to investigate Berry phase effects in solid-state physics [9]. Highly circularly polarized photoluminescence (PL) reported for WSe_2 [10,11], MoS_2 [12–15], and WS_2 [16] confirms efficient and robust optical valley polarization initialization. An important step to test the valley index as a potential information carrier is to demonstrate coherent manipulation of arbitrary valley states with linearly and eventually elliptically polarized laser light. Excitation with linearly polarized light yields the coherent superposition of exciton pseudospin states (optical alignment of excitons) [17]. As each exciton state in ML TMDCs is built from electrons and holes from the K^+ and K^- valleys, optically aligned exciton states are also referred to as coherent valley states, so far only clearly demonstrated in ML WSe_2 [10,11]. In this Letter, we demonstrate how and why valley coherence can be generated efficiently with optical excitation more than 100 meV above the exciton ground state ($1s$). In most semiconductor systems, (pseudo)spin coherence is lost during energy relaxation involving scattering events. As a consequence, strictly resonant laser excitation is favored for traditional coherent control schemes [18–20]. For generation of valley coherences in ML WSe_2, we capitalize on a multiphonon resonance that we uncover in double resonant Raman scattering [21–25]. The double resonance relies on well-defined exciton states [11,26–35] and the strong interaction of excitons with phonons [36–40]. The multiphonon resonance ensures efficient energy relaxation with minimal loss of coherence between the optically generated $2s/2p$ state and the emitting $1s$ state. We observe that the exciton PL emission from coherent valley states is superimposed on a strong double resonant Raman scattering signal (not linked to valley physics) as the incoming and outgoing photon energies are in resonance with the $2s$ and $1s$ exciton states, respectively. Double resonant Raman scattering is a very sensitive tool for investigating the electronic transitions in graphene, graphite, and carbon nanotubes [23–25]. Our results open up possibilities for in-depth studies of the symmetry and energy spacing of the exciton resonances that dominate the optical properties of ML TMDCs, still openly debated in the literature [11,26–35].

Samples and Experimental Setup.—The WSe_2 ML flakes are obtained by micromechanical cleavage of a bulk crystal on SiO_2/Si substrates. Experiments at $T = 4$ K are carried out in a confocal microscope [41]. The detection spot diameter is ≈ 1 μm, i.e., considerably smaller than the ML size of $\sim 10 \times 10$ μm. For time integrated experiments, the PL emission is dispersed in a spectrometer and detected with a Si-CCD camera. Our target is to distinguish between

PL emission and spectrally narrow Raman signals. The WSe_2 ML is therefore excited by *picosecond* pulses generated by a tunable frequency-doubled optical parametric oscillator (OPO) synchronously pumped by a mode-locked Ti:Sa laser. The typical pulse temporal and spectral widths are 1.6 ps and 3 meV, respectively, the latter being smaller than the exciton PL emission linewidth ~15 meV; the repetition rate is 80 MHz.

Results and Discussion.—In our measurements with a tunable laser source, we change the excitation energy and monitor the PL emission of the WSe_2 ML. We concentrate here on the emission of the neutral exciton X^0 ground state ($1s$) at 1.75 eV, with a FWHM of about ~15 meV, see Fig. 1(a). At 1.72 eV, we observe the charged exciton emission (trion, T). The emission observed at lower energies is probably related to localized states, it disappears when the temperature is raised [41]. In previous work [11], we have identified the position of the $2s$ and the $2p$ exciton states in one-photon and two-photon PL excitation (PLE) experiments, respectively. Interestingly, in ML WSe_2, both states are very close in energy (around 1.89 eV). Here, we show in addition hot luminescence of the $2s$ state in Fig. 1(a) as a result of resonant two-photon excitation of the $3p$ state at about 2.03 eV. Crucially for the experiments presented here, resonant excitation of the excited $(2s/2p)$ exciton state results in a strong enhancement of the $1s$ exciton PL. Importantly, using a linearly polarized laser to excite the $2s/2p$ state, the resulting $1s$ emission is strongly linearly polarized ~40% (compare intensities in Fig. 1(d) vs Fig. 1(e) and data for one-photon PLE in the Supplemental Material [42]), a clear fingerprint of efficient valley coherence generation, i.e., exciton alignment [10]. It is very surprising to observe the recombination of a coherent superposition of valley states using optical excitation as high as 140 meV above the $1s$ state as used also for the pioneering demonstration of valley coherence generation in ML WSe_2 [10]. Our two-photon PLE experiments shown in Figs. 1(b)–1(e) clearly demonstrate that the variation of the excitation laser energy has several effects on photons emitted at the $1s$ energy: (i) excitation close to the $2p$ exciton results in drastic changes of the X^0 PL emission intensity (ii) as the laser is scanned through the $2p$ resonance, the line shape and central energy of the emission are modified. Equivalent results for one-photon PLE are shown in the Supplemental Material [42]. A detailed analysis of the shape and energy position of the X^0 emission for different laser energies is shown in Fig. 2(a) for one-photon PLE. When exciting close to the $2s$ resonance, the emission consists of *two* distinct features: In addition to the strong and highly polarized X^0 emission (energy position confirmed for more than 50 values of nonresonant laser excitation energies), we observe a spectrally much narrower feature, that changes energy as the laser energy is changed. Careful fitting of the emission for different laser energies confirms that the additional, narrow feature is observed exactly 140 meV

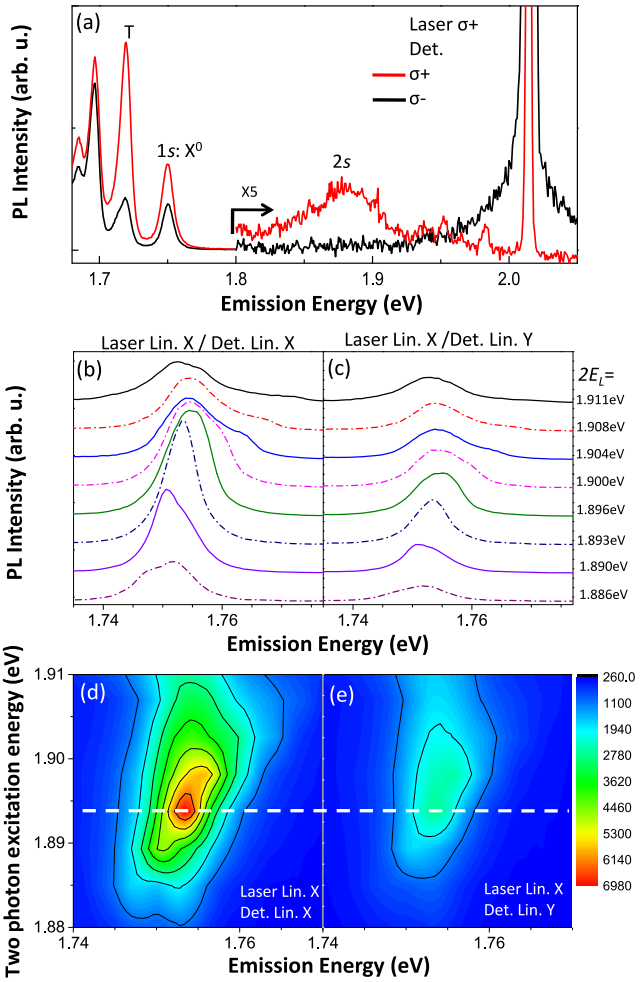

FIG. 1 (color online). *Two-photon excitation* (a) Broad $2s$ exciton PL peak following excitation of $3p$ state. Trion (T) and neutral exciton X^0 (1s) are marked. (b) emission at the X^0 energy ($1s$ exciton) for different laser energies $2E_L$ close to the $2p$ exciton resonance. Laser polarization linear X, detection linear X (copolarized). (c) same as (b) but for detection linear Y (cross polarized). (d) same data as (b) but presented as a contour plot to show changes in PL intensity and shape as a function of $2E_L$, dashed line marks $2p$ resonance. (e) same data as (c), same color scale as (d).

below the laser excitation energy, as shown clearly in Fig. 2(b). In Fig. 2(e), we show that the linewidth of the X^0 PL emission is about 15 meV and the narrower contribution has a FWHM of about 5 meV [46]. We have confirmed this observation in several samples. In Fig. 2(c), we show additional evidence for a different sample: using two-photon excitation, we also find a strong resonance when twice the laser energy $2E_L$ is 140 meV above the $1s$ exciton. Again we analyze the X^0 emission around this resonance: two features, one moving with the laser energy the other one not, can be discerned. Fitting the results in Fig. 2(c) clearly reveals a narrow feature that is always 140 meV below $2E_L$, in addition to the X^0 PL with fixed emission energy, see Fig. 2(d).

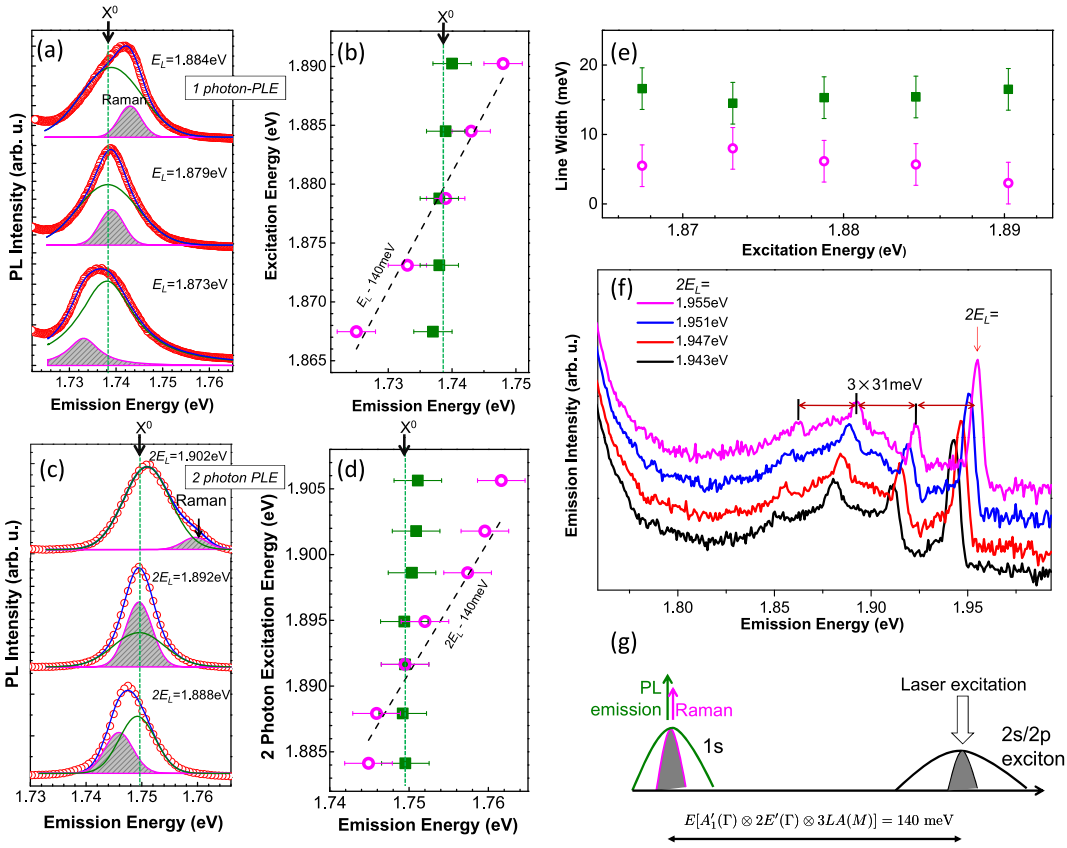

FIG. 2 (color online). One ML WSe_2, $T = 4$ K. (a) emission at exciton X^0 $1s$ energy (red circles) for different excitation laser energies E_L for sample 1, spectra are offset for clarity. Two contributions can be separated via fitting: The X^0 PL component (green) and the resonant Raman contribution (pink, shaded grey), the latter changes with E_L from top to bottom panel. (b) Extracted transition energies for X^0 PL (green squares) are constant, resonant Raman spectral position (open circles) changes linearly as a function of laser excitation energy, for comparison, we plot $E_L - 140$ meV (dashed line). (c) and (d) same as (a) and (b) but using two-photon excitation for sample 2. (e) Linewidth of the X^0 PL (green squares) and resonant Raman signal (pink circles) as a function of laser excitation energy as extracted from panel (a). (f) Simply resonant Raman scattering as outgoing photons are in resonance with the broad $2s$ exciton state shows three phonon replica more than 90 meV below the two-photon excitation. (g) Schematics of exciton generation and relaxation via multiple phonon processes, leading to enhanced X^0 emission and a double resonance (incoming and outgoing photons) for Raman scattering.

What is the physical origin of the spectrally narrow peak whose energy is fixed with respect to that of the laser? Why are the X^0 coherence and emission intensity at a maximum when this narrow peak centre energy is exactly at the X^0 $1s$ resonance? A maximum in the PLE signal requires (a) strong absorption by an excited state, here the $2s$ or $2p$ exciton, and (b) efficient relaxation from the excited state to the exciton ground state ($1s$). Relaxation between electronic states in semiconductors is most efficient by emission of phonons. In addition, this allows to partially preserve coherence [47]. Raman studies in ML TMDC have revealed a multitude of prominent phonon modes, e.g., see [36–39,48–52]. A key point in our experiment is the enhancement of light scattering by phonons as the photon energy is in resonance with an electronic transition. In Fig. 2(f), we present an example of resonant Raman scattering in our sample, using a single (not double) resonance, similar to recent experiments in ML MoS_2 [36]: Excitons are generated via two-photon absorption, and up to three optical phonons (with energy 31 meV [53]) are emitted, so that excitonic final states fall into the broad line of the $2s/2p$ state. This simple resonant Raman experiment shows *three* clear phonon replica more than 90 meV below the excitation energy. Multiple Raman features are often observed in 2D materials [37,54] as the interaction of phonons with exciton transitions is efficient. Due to 2D confinement, exciton oscillator strength and binding energy are enhanced and emission linewidths in the meV range allow us to see clear resonance effects. For $2s/2p$ to $1s$ phonon-assisted transitions investigated here in ML WSe_2, an ideal situation for *double* resonant Raman scattering

TABLE I. Selected phonon energies in WSe_2, after Ref. [37].

Mode	Raman shift [cm^{-1}]	Energy [meV]
$E'(\Gamma)$	248	30.73
$A_1'(\Gamma)$	250	30.98
$3LA(M)$	394	48.82

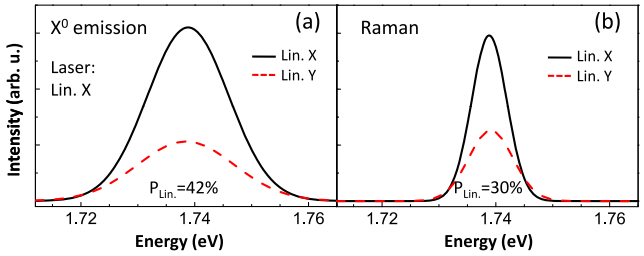

FIG. 3 (color online). (a) Following linearly polarized laser excitation 140 meV above the X^0 PL emission energy, the PL is strongly polarized. (b) The narrower double Raman resonance is also strongly linearly polarized. The sum of the graphs shown in (a) and (b) is a least square fit for the global emission with Gaussian line shapes. We plot them here in different panels for clarity.

occurs: The incoming photons are in resonance with the $2s/2p$ exciton state and the outgoing photons with the $1s$ exciton state, see Fig. 2(g). Double resonant Raman scattering is extremely efficient as the scattering cross sections are strongly enhanced [21,22,55–57], see model description in Supplemental Material [42].

Our next target is to analyze which phonon modes can be combined to bridge the 140 meV energy difference between the $2s/2p$ and $1s$ exciton states, respecting the wave vector conservation and symmetry (see Supplemental Material for details [42]). The WSe_2 monolayer has D_{3h} point symmetry and $P\bar{6}m2$ (187 or D^1_{3h}) space group. The analysis of Refs. [48–50,58] allows us to associate nine phonon modes at the Γ point (center of the Brillouin zone) with the following representations of D_{3h} point group: $A_1' + 2A_2'' + 2E' + E''$. To be Raman active, the phonon modes should transform as quadratic combinations of coordinates, i.e., according to the irreducible representations A_1', E', and E'' [42]. Theoretical calculations of phonon energies in WSe_2 monolayers are presented in Refs. [50,51] and peaks in Raman spectra are identified in Refs. [37,52], with strong signals with well defined peaks attributed to the $A_1'(\Gamma)$, $E'(\Gamma)$, and $3LA(\mathrm{M})$ modes. The combinations of the prominent phonons $A_1'(\Gamma) \otimes 2E'(\Gamma) \otimes 3LA(\mathrm{M})$, or $2A_1'(\Gamma) \otimes E'(\Gamma) \otimes 3LA(\mathrm{M})$, or $3A_1'(\Gamma) \otimes 3LA(\mathrm{M})$, or $3E'(\Gamma) \otimes 3LA(\mathrm{M})$ [59] have an energy of $\hbar\omega \approx 140$ meV, see Table I. This is very close to the energy separation between $2s/2p$ and $1s$ excitons in ML WSe_2 and can account for double resonant Raman scattering [42]. These combinations contain the modes transforming both according to A_1' and E' and, hence, are Raman active in $\bar{z}(xx)z$ and in $\bar{z}(xy)z$ configurations, i.e., both in co- and cross-linear polarizations. Analysis shows that these multiphonon modes are consistent with both resonant Raman transitions from $2s$ to $1s$ and from $2p$ to $1s$ exciton states observed, respectively, in one-photon and two-photon excitation experiments [42].

Our detailed analysis of double resonant Raman scattering allows us to distinguish between the different contributions to the ML WSe_2 emission following excitation with linearly polarized laser light [60]. As we can spectrally separate the X^0 PL from the Raman signal, we can analyze the polarization of each contribution individually, as shown in Fig. 3. For a laser energy 140 meV above the X^0 PL energy, we observe a maximum of the global emission intensity, but also for each of the two components taken individually. For the X^0 emission, we observe a linear polarization degree of 42%, corresponding to strong valley coherence, i.e., exciton alignment. From this time integrated measurement, we can infer that the coherence is maintained during the PL emission time that we have determined to be in the ps range [41]. For the Raman signal, we observe a linear polarization degree of 30%. The depolarization of Raman line is qualitatively in agreement with the selection rules for the relevant modes, see above.

Conclusions.—The optical generation of valley coherence using laser excitation more than 100 meV above the exciton ground state opens up fascinating prospects for coherent valley index manipulation. Our results uncover the physical processes involved in efficient valley coherence generation that we detect via the linear polarization degree of the $1s$ exciton PL. Excitons are efficiently generated tuning the laser in resonance with the $2s/2p$ exciton states. In double resonant Raman experiments, we show that the $2s/2p$ states are separated from the $1s$ state by a phonon multiple. This allows for efficient energy relaxation $2p/2s \rightarrow 1s$ with, very importantly, minimal loss of coherence. This might be one of the reasons why efficient valley coherence can be generated in ML WSe_2 contrary to MoS_2 or $MoSe_2$. In particular, we do not observe the double resonant Raman feature in two-photon PLE experiments on high quality $MoSe_2$ MLs around the $2p$ resonance [61], as can be clearly seen in Fig. S2 of the Supplemental Material [42]. Tuning of the separation of the exciton levels in different ML TMDCs can be achieved by altering the dielectric environment (screening) [30] or applying strain and external fields. Our work suggests that aiming for level separations that correspond to multiphonon resonances can be envisaged as a route towards achieving higher valley coherence in different ML TMDC materials. Further theoretical work is needed to reveal the nature (perturbative or strongly coupled) of the exciton-phonon interaction [62]. Also the influence of magnetic fields applied perpendicular to the sample plane will allow us to study separately the evolution of the polarization of the Raman signal and the valley coherence of the neutral exciton [63,64].

We acknowledge funding from ERC Grant No. 306719, ANR MoS2ValleyControl. M. M. G. is grateful to Labex NEXT for an invited Professorship, RFBR, RF President Grant No. MD-5726.2015.2, and the Dynasty Foundation.

[1] K. F. Mak, C. Lee, J. Hone, J. Shan, and T. F. Heinz, Phys. Rev. Lett. **105**, 136805 (2010).
[2] A. Splendiani, L. Sun, Y. Zhang, T. Li, J. Kim, C.-Y. Chim, G. Galli, and F. Wang, Nano Lett. **10**, 1271 (2010).

[3] W. Zhao, Z. Ghorannevis, L. Chu, M. Toh, C. Kloc, P.-H. Tan, and G. Eda, ACS Nano **7**, 791 (2013).

[4] F. Withers, O. Del Pozo-Zamudio, A. Mishchenko, A. Rooney, A. Gholinia, K. Watanabe, T. Taniguchi, S. Haigh, A. Geim, A. Tartakovskii *et al.*, Nat. Mater. **14**, 301 (2015).

[5] D. Xiao, G.-B. Liu, W. Feng, X. Xu, and W. Yao, Phys. Rev. Lett. **108**, 196802 (2012).

[6] T. Cao, G. Wang, W. Han, H. Ye, C. Zhu, J. Shi, Q. Niu, P. Tan, E. Wang, B. Liu *et al.*, Nat. Commun. **3**, 887 (2012).

[7] K. F. Mak, K. L. McGill, J. Park, and P. L. McEuen, Science **344**, 1489 (2014).

[8] X. Xu, D. Xiao, T. F. Heinz, and W. Yao, Nat. Phys. **10**, 343 (2014).

[9] D. Xiao, M.-C. Chang, and Q. Niu, Rev. Mod. Phys. **82**, 1959 (2010).

[10] A. M. Jones, H. Yu, N. J. Ghimire, S. Wu, G. Aivazian, J. S. Ross, B. Zhao, J. Yan, D. G. Mandrus, D. Xiao *et al.*, Nat. Nanotechnol. **8**, 634 (2013).

[11] G. Wang, X. Marie, I. Gerber, T. Amand, D. Lagarde, L. Bouet, M. Vidal, A. Balocchi, and B. Urbaszek, Phys. Rev. Lett. **114**, 097403 (2015).

[12] K. F. Mak, K. He, J. Shan, and T. F. Heinz, Nat. Nanotechnol. **7**, 494 (2012).

[13] H. Zeng, J. Dai, W. Yao, D. Xiao, and X. Cui, Nat. Nanotechnol. **7**, 490 (2012).

[14] G. Kioseoglou, A. T. Hanbicki, M. Currie, A. L. Friedman, D. Gunlycke, and B. T. Jonker, Appl. Phys. Lett. **101**, 221907 (2012).

[15] G. Sallen, L. Bouet, X. Marie, G. Wang, C. R. Zhu, W. P. Han, Y. Lu, P. H. Tan, T. Amand, B. L. Liu *et al.*, Phys. Rev. B **86**, 081301 (2012).

[16] B. Zhu, H. Zeng, J. Dai, Z. Gong, and X. Cui, Proc. Natl. Acad. Sci. U.S.A. **111**, 11606 (2014).

[17] *Optical Orientation*, edited by F. Meier and B. Zakharchenya, Modern Problems in Condensed Matter Sciences Vol. 8 (North-Holland Physics Publishing, Amsterdam, 1984).

[18] *Spin Physics in Semiconductors*, edited by M. Dyakonov, Springer Series in Solid-State Science Vol. 157 (Springer-Verlag, Berlin, 2008).

[19] A. Greilich, S. E. Economou, S. Spatzek, D. Yakovlev, D. Reuter, A. Wieck, T. Reinecke, and M. Bayer, Nat. Phys. **5**, 262 (2009).

[20] X. Marie, P. Le Jeune, T. Amand, M. Brousseau, J. Barrau, M. Paillard, and R. Planel, Phys. Rev. Lett. **79**, 3222 (1997).

[21] R. Miller, D. Kleinman, and A. Gossard, Solid State Commun. **60**, 213 (1986).

[22] F. Cerdeira, E. Anastassakis, W. Kauschke, and M. Cardona, Phys. Rev. Lett. **57**, 3209 (1986).

[23] A. C. Ferrari, J. C. Meyer, V. Scardaci, C. Casiraghi, M. Lazzeri, F. Mauri, S. Piscanec, D. Jiang, K. S. Novoselov, S. Roth *et al.*, Phys. Rev. Lett. **97**, 187401 (2006).

[24] C. Thomsen and S. Reich, Phys. Rev. Lett. **85**, 5214 (2000).

[25] J. Maultzsch, S. Reich, U. Schlecht, and C. Thomsen, Phys. Rev. Lett. **91**, 087402 (2003).

[26] T. Cheiwchanchamnangij and W. R. L. Lambrecht, Phys. Rev. B **85**, 205302 (2012).

[27] H.-P. Komsa and A. V. Krasheninnikov, Phys. Rev. B **86**, 241201 (2012).

[28] Y. Song and H. Dery, Phys. Rev. Lett. **111**, 026601 (2013).

[29] K. He, N. Kumar, L. Zhao, Z. Wang, K. F. Mak, H. Zhao, and J. Shan, Phys. Rev. Lett. **113**, 026803 (2014).

[30] M. M. Ugeda, A. J. Bradley, S.-F. Shi, F. H. da Jornada, Y. Zhang, D. Y. Qiu, S.-K. Mo, Z. Hussain, Z.-X. Shen, F. Wang *et al.*, Nat. Mater. **13**, 1091 (2014).

[31] A. Chernikov, T. C. Berkelbach, H. M. Hill, A. Rigosi, Y. Li, O. B. Aslan, D. R. Reichman, M. S. Hybertsen, and T. F. Heinz, Phys. Rev. Lett. **113**, 076802 (2014).

[32] Z. Ye, T. Cao, K. O'Brien, H. Zhu, X. Yin, Y. Wang, S. G. Louie, and X. Zhang, Nature (London) **513**, 214 (2014).

[33] A. R. Klots, A. K. M. Newaz, B. Wang, D. Prasai, H. Krzyzanowska, D. Caudel, N. J. Ghimire, J. Yan, B. L. Ivanov, K. A. Velizhanin *et al.*, Sci. Rep. **4**, 6608 (2014).

[34] B. Zhu, X. Chen, and X. Cui, Sci. Rep. **5**, 9218 (2015).

[35] A. Hanbicki, M. Currie, G. Kioseoglou, A. Friedman, and B. Jonker, Solid State Commun. **203**, 16 (2015).

[36] B. R. Carvalho, L. M. Malard, J. M. Alves, C. Fantini, and M. A. Pimenta, Phys. Rev. Lett. **114**, 136403 (2015).

[37] X. Zhang, X.-F. Qiao, W. Shi, J.-B. Wu, D.-S. Jiang, and P.-H. Tan, Chem. Soc. Rev. **44**, 2757 (2015).

[38] J.-H. Fan, P. Gao, A.-M. Zhang, B.-R. Zhu, H.-L. Zeng, X.-D. Cui, R. He, and Q.-M. Zhang, J. Appl. Phys. **115**, 053527 (2014).

[39] E. del Corro, H. Terrones, A. Elias, C. Fantini, S. Feng, M. A. Nguyen, T. E. Mallouk, M. Terrones, and M. A. Pimenta, ACS Nano **8**, 9629 (2014).

[40] A. P. S. Gaur, S. Sahoo, J. F. Scott, and R. S. Katiyar, J. Phys. Chem. C **119**, 5146 (2015).

[41] G. Wang, L. Bouet, D. Lagarde, M. Vidal, A. Balocchi, T. Amand, X. Marie, and B. Urbaszek, Phys. Rev. B **90**, 075413 (2014).

[42] See Supplemental Material at http://link.aps.org/supplemental/10.1103/PhysRevLett.115.117401 which includes Refs. [43–45] and contains additional experimental data and a theoretical description of double resonant Raman scattering.

[43] G. Wang, C. Robert, A. Suslu, B. Chen, S. Yang, S. Alamdari, I. C. Gerber, T. Amand, X. Marie, S. Tongay *et al.*, arXiv:1506.08114.

[44] A. Molina-Sánchez and L. Wirtz, Phys. Rev. B **84**, 155413 (2011).

[45] R. M. Martin and C. M. Varma, Phys. Rev. Lett. **26**, 1241 (1971).

[46] Measuring 5 meV and not 3 meV as given by the laser linewidth might be due to broadening by phonon dispersion and damping.

[47] T. Flissikowski, A. Hundt, M. Lowisch, M. Rabe, and F. Henneberger, Phys. Rev. Lett. **86**, 3172 (2001).

[48] S. Jiménez Sandoval, D. Yang, R. F. Frindt, and J. C. Irwin, Phys. Rev. B **44**, 3955 (1991).

[49] C. Ataca, M. Topsakal, E. Aktrk, and S. Ciraci, J. Phys. Chem. C **115**, 16354 (2011).

[50] X. Luo, Y. Zhao, J. Zhang, M. Toh, C. Kloc, Q. Xiong, and S. Y. Quek, Phys. Rev. B **88**, 195313 (2013).

[51] H. Sahin, S. Tongay, S. Horzum, W. Fan, J. Zhou, J. Li, J. Wu, and F. M. Peeters, Phys. Rev. B **87**, 165409 (2013).

[52] W. Zhao, Z. Ghorannevis, K. K. Amara, J. R. Pang, M. Toh, X. Zhang, C. Kloc, P. H. Tan, and G. Eda, Nanoscale **5**, 9677 (2013).

[53] The transition between $2p$ and $1s$ mode is enabled by $E'(\Gamma)$ optical phonon. Two-or three-phonon replicas may involve also $A_1'(\Gamma)$ phonon which is almost degenerate with $E'(\Gamma)$, see Table I and Ref. [37].

[54] J. Reydellet, M. Balkanski, and J. Besson, J. Phys. (Paris), Lett. **37**, 219 (1976).

[55] Peter Y. Yu and Manuel Cardona, *Fundamentals of Semiconductors* (Springer-Verlag, Berlin, Germany, 2010), Chap. 7.

[56] E. L. Ivchenko, *Optical Spectroscopy of Semiconductor Nanostructures* (Alpha Science, Harrow, United Kingdom, 2005).

[57] H. Guo, T. Yang, M. Yamamoto, L. Zhou, R. Ishikawa, K. Ueno, K. Tsukagoshi, Z. Zhang, M. S. Dresselhaus, and R. Saito, Phys. Rev. B **91**, 205415 (2015).

[58] J. Ribeiro-Soares, R. M. Almeida, E. B. Barros, P. T. Araujo, M. S. Dresselhaus, L. G. Cancado, and A. Jorio, Phys. Rev. B **90**, 115438 (2014).

[59] The combination of three acoustic phonons at M point of the Brillouin zone has zero total wave vector and is Raman active [42].

[60] For other semiconductors, this separation can be achieved in time-resolved experiments, as the scattered light is only present during the laser pulse, whereas the PL signal persists for longer. This is not possible here as the PL signal decays within ps, *i.e.*, during the excitation pulse of our ps laser, here experiments with fs time resolution would be helpful. Although the same physical processes analyzed in this work will be applicable to experiments with femtosecond laser pulses, in the spectral domain, the Raman signal will appear much broader than the PL linewidth and will not be separable.

[61] G. Wang, I. C. Gerber, L. Bouet, D. Lagarde, A. Balocchi, M. Vidal, E. Palleau, T. Amand, X. Marie, and B. Urbaszek, arXiv:1504.06333.

[62] O. Verzelen, R. Ferreira, and G. Bastard, Phys. Rev. Lett. **88**, 146803 (2002).

[63] G. Aivazian, Z. Gong, A. M. Jones, R.-L. Chu, J. Yan, D. G. Mandrus, C. Zhang, D. Cobden, W. Yao, and X. Xu, Nat. Phys. **11**, 148 (2015).

[64] G. Wang, L. Bouet, M. M. Glazov, T. Amand, E. L. Ivchenko, E. Palleau, X. Marie, and B. Urbaszek, 2D Materials **2**, 034002 (2015).